



**HAL**  
open science

## MHD modeling of rotating arc under restrike mode: dynamics and stability

Papa Gueye, Yann Cressault, Vandad-Julien Rohani, Laurent Fulcheri

► **To cite this version:**

Papa Gueye, Yann Cressault, Vandad-Julien Rohani, Laurent Fulcheri. MHD modeling of rotating arc under restrike mode: dynamics and stability. 23rd International Symposium on Plasma Chemistry, Jul 2017, Montréal, Canada. hal-01524618

**HAL Id: hal-01524618**

**<https://minesparis-psl.hal.science/hal-01524618>**

Submitted on 18 May 2017

**HAL** is a multi-disciplinary open access archive for the deposit and dissemination of scientific research documents, whether they are published or not. The documents may come from teaching and research institutions in France or abroad, or from public or private research centers.

L'archive ouverte pluridisciplinaire **HAL**, est destinée au dépôt et à la diffusion de documents scientifiques de niveau recherche, publiés ou non, émanant des établissements d'enseignement et de recherche français ou étrangers, des laboratoires publics ou privés.

# MHD modeling of rotating arc under restrike mode: dynamics and stability

P. GUEYE<sup>1</sup>, Y. Cressault<sup>2</sup>, V. Rohani<sup>1</sup>, L. Fulcheri<sup>1</sup>

<sup>1</sup>PERSEE, MINES ParisTech, PSL-Research University, France

<sup>2</sup>LAPLACE, University of Toulouse UPS, France

**Abstract:** This paper focuses on the 3D MHD modeling on an arc plasma in a Kvaerner-type torch made of two concentric electrodes. The spots are displaced with an external magnetic field. We observe different phenomenologies in arc movement, ranging from a gliding arc on the electrodes surfaces to jumping arc foot. The former mode induces a lower heat flux at the electrodes surfaces in comparison to the latter. Besides those dynamics which are indebted to gas nature, current and flow rates, arc stability is also investigated with a theoretical model based on an energy principle.

**Keywords:** MHD, Kvaerner-type torch, rotating arc dynamics, hop-off mode

## 1. Introduction

In plasma torches, arc dynamics is of great importance as it impacts design, heat flux distribution, power and stability control. Those dynamics are particularly indebted to the torch configuration, especially for magnetically driven electrodes where different modes of arc-foot attachment and movement can occur. They range from the smoothly rotating arc foot that distributes the heat flux uniformly around the circumference of the electrodes to the jumping arc foot, where the arc foot either repeatedly visits certain spots on the electrode surface or follow a random process. In this paper we present MHD modeling of an hydrogen arc in a Kvaerner-type torch where electrodes are concentric. Details regarding this torch development can be found in [1]. The arc roots are displaced with an external magnetic field. A very striking arc phenomenology was observed, depending on operational conditions. The arc dynamics on electrodes surfaces is carefully described; we discuss also its stability by means of a mathematical model based on energy principle. It is shown that, under the two concentric electrodes configuration, pressure-driven instability causes deformation of the stretched arc besides its tilting toward electrodes surface.

## 2. Mathematical models

Under the local thermodynamic equilibrium (LTE) assumption, a one-temperature model is used despite deviations from the equilibrium at the arc fringes and near the electrodes. The plasma is considered optically thin, the flow as laminar and incompressible. The anodic and cathodic sheaths are not considered whereas plasma/electrodes interfaces is of importance and treated with the approach presented in the section 3. Indeed, reasonably accurate calculations of arc properties can be made assuming LTE and omitting diffusion effects, provided that mesh sizes at the electrodes are  $\sim 0.01$ - $0.04$  cm. This

distance is approximately the 'diffusion length' of electrons in the arc plasma. Such approach called the 'LTE-diffusion approximation' [2] is followed in this paper.

Then the flow of a thermal plasma can be fully described by five independent variables, chosen as :  $p$  pressure,  $\vec{u}$  velocity,  $T$  temperature,  $\phi$  electric potential and  $\vec{A}$  magnetic potential vector . They form the vector

$$\mathbf{Y} = [p \quad \vec{u} \quad T \quad \phi \quad \vec{A}]^t \quad (1)$$

where the subscript t indicates *transpose*. The set of equations describing a thermal plasma flow can be expressed in a compact form as a system of *transient-advective-diffusive-reactive* (TADR) equations as

$$\mathbf{R}(\mathbf{Y}) = \mathbf{A}_0 \partial \mathbf{Y} / \partial t + (\mathbf{A} \cdot \nabla) \mathbf{Y} - \nabla \cdot (\mathbf{K} \nabla \mathbf{Y}) - (\mathbf{S}_1 \mathbf{Y} + \mathbf{S}_0) = \mathbf{0} \quad (2)$$

where  $\mathbf{R}$  represents the vector of residuals and  $\mathbf{A}_0$ ,  $\mathbf{A}$ ,  $\mathbf{K}$ ,  $\mathbf{S}_1$  and  $\mathbf{S}_0$  are matrices of appropriate sizes. Under this formulation, the MHD equations are presented in Table 1.  $\rho$  represents mass density,  $t$  time,  $\mu$  dynamic viscosity,  $\vec{\delta}$  the identity tensor  $\vec{J}_q$  current density,  $\vec{B}$  magnetic field,  $C_p$  specific heat at constant pressure,  $\kappa$  thermal conductivity,  $h_e$  electron enthalpy,  $\vec{J}_e$  mass diffusion flux of electrons,  $\vec{E}$  electric field,  $\dot{Q}_r$  volumetric radiation losses,  $\sigma$  electrical conductivity,  $e$  the elementary charge and  $\mu_0$  the permeability of free space.

Radiation is calculated using the net emission coefficient  $\epsilon_r$  [3]. Its derivation requires the spectrum of the absorption coefficient  $k'_v$ . This is achieved thanks to the recent work of T. Billoux [4]. It yields to a huge database with a temperature range from 300 to 30 000 K and wavelengths from  $0.209 \mu\text{m}$  to infrared, as shown in figure 1.

$$\dot{Q}_r = 4\pi\epsilon_r = 4\pi \int_0^\infty k'_v B_v \exp(-k'_v R_p) dv \quad (3)$$

i	$Y_i$	Transient	Advective	Diffusive	Reactive
1	$p$	$\frac{\partial p}{\partial t}$	$\nabla \cdot \rho \vec{u}$	0	0
2	$\vec{u}$	$\rho \frac{\partial \vec{u}}{\partial t}$	$\rho \vec{u} \cdot \nabla \vec{u} - \nabla p$	$\nabla \cdot \mu (\nabla \vec{u} + \nabla \vec{u}^t - \frac{2}{3} \nabla \cdot \vec{u} \vec{\delta})$	$\vec{J}_q \times \vec{B} + \rho \vec{g}$
3	$T$	$\rho C_p \frac{\partial T}{\partial t}$	$\rho C_p \vec{u} \cdot \nabla T$	$\nabla \cdot (\kappa \nabla T + \frac{5}{2} k_B T_e \frac{\vec{J}_q}{e})$	$\vec{J}_q \cdot (\vec{E} + \vec{u} \times \vec{B}) - \dot{Q}_r$
4	$\phi$	0	0	$\nabla \cdot \sigma (\nabla \phi - \vec{u} \times \nabla \times \vec{A})$	0
5	$\vec{A}$	$\frac{\partial \vec{A}}{\partial t}$	$\nabla \phi - \vec{u} \times \nabla \times \vec{A}$	$(\mu_0 \sigma)^{-1} \nabla^2 \vec{A}$	0

Table 1: Thermal plasma equations: *transient + advective - diffusive - reactive = 0*

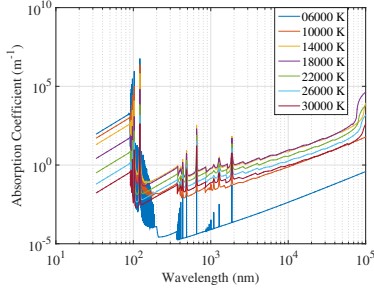


Figure 1: Absorption coefficient of  $H_2$  at 1 bar

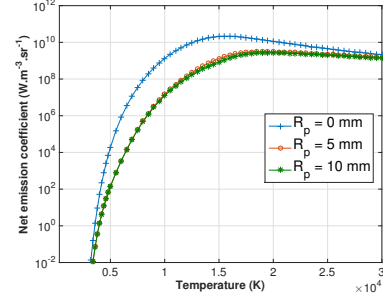


Figure 2: NEC of  $H_2$  at 1 bar and for different  $R_p$

The radiation from background continuum, either molecular ( $H_2$ ) or atomic ( $H$ ,  $H^-$  and  $H^+$ ), from molecular diatomic bands, and from 74 lines spectrum for hydrogen is considered. Such huge investigation allows having a more precise calculation of the radiative contribution. The electric and magnetic potentials are related to the electric and magnetic fields and the current density through the following expressions

$$\vec{E} = -\nabla\phi - \frac{\partial \vec{A}}{\partial t}, \quad \vec{B} = \nabla \times \vec{A}, \quad \vec{J}_q = \sigma(\vec{E} + \vec{u} \times \vec{B}) \quad (4)$$

The thermodynamic and transport properties appearing in Table 1 are computed using TT Winner code [5] based on the Gibbs free energy minimization, with the temperature ranging from 300 K to 20 000 K.

### 3. Computational domain and boundary conditions

The calculation domain is based on a Kvaerner-type torch composed of a plasma zone and a post-discharge zone. The torch consists of two concentric graphite electrodes, schematically shown in Fig. 3. The grid mesh of 1/8 of the domain realized using SALOME 5.1.4 [6] contains 6.7 millions hexa-cells and is refined at the post-discharge zone, in particular near the electrodes. The boundary conditions are detailed in Table 2. To improve arc/electrodes thermal transfer, the graphite electrodes are incorporated into the computational domain [7]. The methodology used to integrate the solid phase in a fluid mechanics model was entirely based on the work of Borel [8].

This step is not inconsequential, as it involves removing the diffusivity from the material/fluid faces. Gradient reconstruction in the solid/fluid interface is removed and the continuity of thermophysical properties is calculated by harmonic interpolations. The arc voltage  $\phi = dpot$  is calculated at each time step to satisfy the current set boundary condition at the cathode.

The coupled Navier-Stokes and Maxwell's equations are solved using the CFD software Code Saturne V2.0.1 based on a co-located finite volume, on the SIMPLEC algorithm and a fully implicit solution of equations [9]. The time step is set to 2  $\mu s$ . The external coil is accounted for, through a source term in the Navier-Stokes equation. The external field has two components: radial and axial components,  $B_r = -4$  mT and  $B_z = 40$  mT respectively.

To enable re-arcng, the hot gas column reattachment model developed by Baudry et al [10] is used. The stretching of the arc column leads to an increase of the voltage drop, and therefore the electric field, between the arc column fringes and the cathode surface. The breakdown occurs when the electric field overcomes a specified threshold value of the electric field, named  $E_b$ , in a cell of the computational mesh. When the critical value  $E_b$ , the boundary conditions on the cathode potential are modified to force the new arc root to connect to the closest point of the cathode. Short circuit is imposed with the creation of a new conducting channel.

### 4. Results and discussions

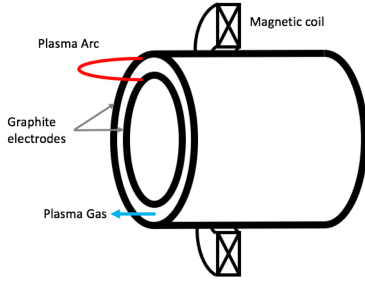


Figure 3: Schematic of the Kvaerner-type torch

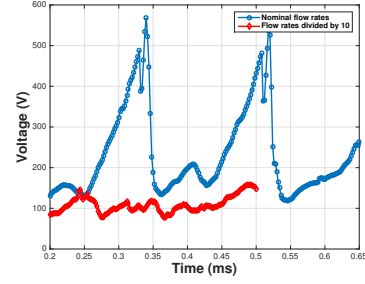


Figure 4: Voltage 1 bar, 1000 A,  $E_b = 1e5$  V/m

$\bar{Y}_i$	Inlets	Cathode	Anode	Walls	Outlet
$p$	$p_{,n} = 0$	$p_{,n} = 0$	$p_{,n} = 0$	$p_{,n} = 0$	$p = p_{out}$
$\vec{u}$	$\vec{u} = \vec{u}_{in}$	$u_i = 0$	$u_i = 0$	$u_i = 0$	$u_{i,n} = 0$
$T$	$T = T_{in}$	$T = T_{in}$	$T = T_{in}$	$T_{,n} = 0$	$T_{,n} = 0$
$\phi$	$\phi_{,n} = 0$	$\phi_{,n} = 0$	$\phi = dpot$	$\phi_{,n} = 0$	$\phi_{,n} = 0$
$\vec{A}$	$A_{i,n} = 0$	$A_{i,n} = 0$	$A_{i,n} = 0$	$A_{i,n} = 0$	$A_i = 0$

Table 2: Boundary conditions:  $a_{,n} = \partial a / \partial n$  differentiation in the direction of the outer normal to the boundary;  $i = x, y, z$  Cartesian coordinates

The MHD modeling results enlightens very particular dynamics inside this Kvaerner-type torch. Under the nominal operating conditions, arc displacement is indeed observed to be a halted process. The external magnet causes the tilting of the stretched arc towards the electrodes surfaces. Consequently the properties are locally modified; the restrike breakdown condition is met and a new arc is created at this new location. The overall movement is a jumping arc and we speak of hop-off mode, well shown in Fig. 5. Another remarkable feature under this mode is the following: the arc previous locations can have a great impact on the heat prehistory of the electrodes [11] and consequently on its dynamics. Arc wake represents the cold boundary layer and where the breakdown condition can be satisfied. This explains why re-arcing can occur backward to the initial rotational direction. Such jumping mode is possible because the arc may prefer to attach on a location that has been preheated, owing to a previous visitation by the arc foot. Moreover, it appears that the axial gas flow, not only impacts the arc rotational velocity as observed in many configurations but also controls the dynamics of the arc on electrodes surfaces. Reducing the latter by 10 have led to a shift in the dynamics mode: a gliding arc is observed on Fig. 6, corresponding to a lower voltage (Fig. 4) due to a hotter and more importantly shorter arc.

## 5. Conclusion

This paper highlights the particular dynamics modes and their stability inside a Kvaerner-type torch. The outcomes are in

agreement with experimental observations. The model gives crucial information regarding the design, the control and the optimization of torch operation.

## References

- [1] J. A. Bakken et al. *Pure Appl. Chem.*, 70(6):1223–1228, 1998.
- [2] J. J. Lowke and M. Tanaka. *Journal of Physics D-Applied Physics*, 39(16):3634–3643, 2006.
- [3] J. J. Lowke. *Journal of Quantitative Spectroscopy And Radiative Transfer*, 14(2):111–122, 1974.
- [4] T. Billoux, Y. Cressault, and A. Gleizes. *Journal of Quantitative Spectroscopy and Radiative Transfer*, 166:42–54, November 2015.
- [5] B. Pateyron. Thesis, Université de Limoges, 1987.
- [6] <http://www.salome-platform.org/>.
- [7] M. Tanaka, H. Terasaki, M. Ushio, and J. J. Lowke. 23(3):585–606, 2003.
- [8] D. Borel. Thesis, Université de Rouen, 2013.
- [9] F. Archambeau. *Int. J. Finite Volume*, 1(1), 2004.
- [10] C. Baudry, A. Vardelle, and G. Mariaux. *High Temperature Material Processes*, 9(1):1–15, 2005.
- [11] V. Nemchinsky. *Plasma Sources Science Technology*, 24(3), 2015.

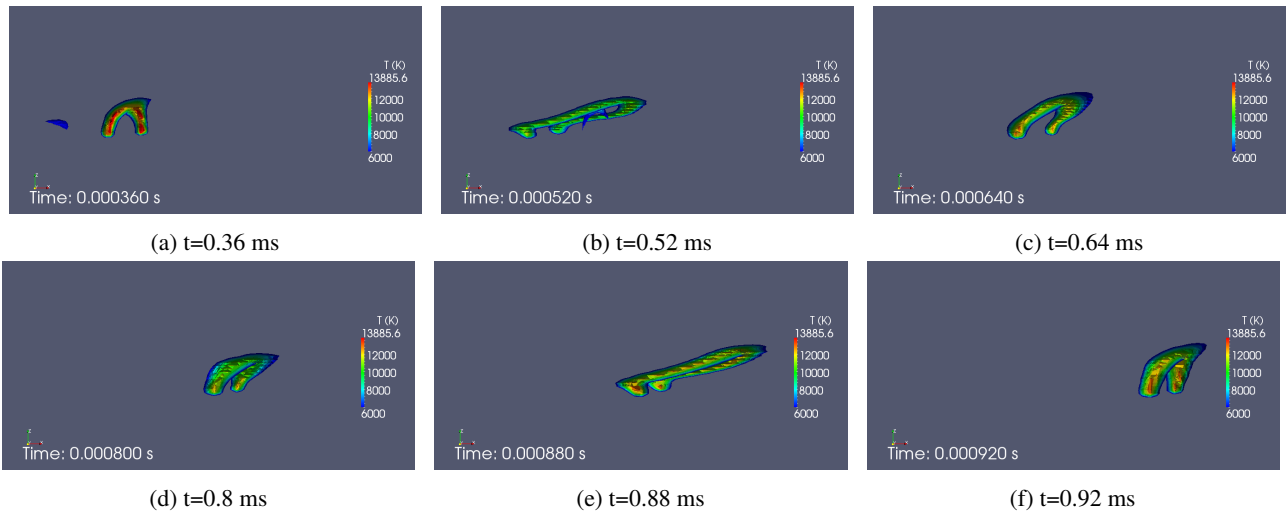


Figure 5: Time sequence of the PBR arc (side view): Hydrogen, 1 bar, 1000 A,  $B_r = -4$  mT,  $B_z = 40$  mT and  $E_b=1e5$  V/m

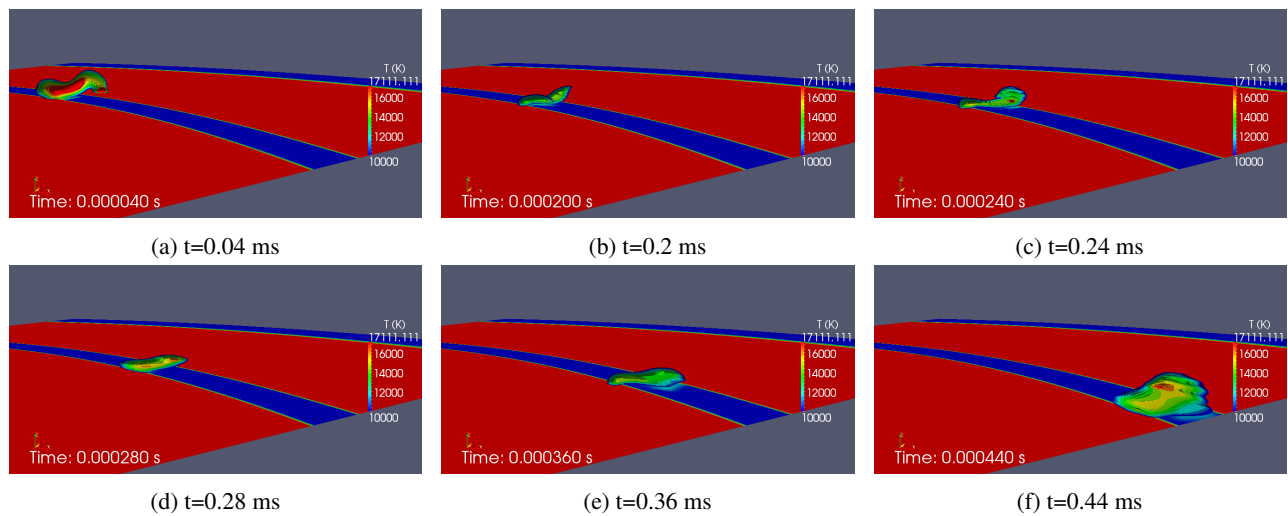


Figure 6: Time sequence of the PBR arc (side view): Hydrogen, 1 bar, 1000 A,  $B_r = -4$  mT,  $B_z = 40$  mT and  $E_b=1e5$  V/m with nominal flow rates reduced by 10

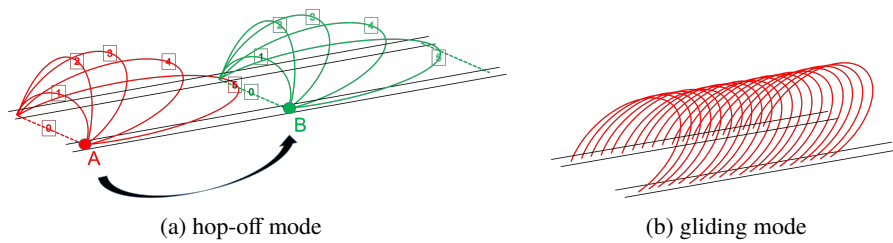


Figure 7: Schematic decomposition of observed arc dynamics: for the hope-off mode  $0 \Rightarrow 1 \Rightarrow 2$  "stretching",  $2 \Rightarrow 3 \Rightarrow 4 \Rightarrow 5$  "tilting",  $0 \Rightarrow$  "restriking"